Proceedings of The Thirteenth (2003) International Offshore and Polar Engineering Conference
Honolulu, Hawaii, USA, May 25−30, 2003

ISBN 1−880653-60−5 (Set); ISSN 1098−6189 (Set)

Computations of Three-Dimensional Overturning Waves in Shallow Water: Dynamics and Kinematics

P. Guyenne[1] *and S.T. Grilli*[2]

[1] Department of Mathematics, McMaster University, Hamilton, ON, Canada

[2] Department of Ocean Engineering, University of Rhode Island, Narragansett, RI, USA

ABSTRACT

Simulations in a three-dimensional numerical wave tank are performed to investigate the shoaling and breaking of a solitary wave over a sloping ridge with a lateral modulation. The model is based on a high-order boundary element method combined with a mixed Eulerian–Lagrangian formulation. Our study is focused on the case of a plunging breaker and is aimed at describing the phenomenon of wave overturning in shallow water. A local regridding technique is developed to allow computations to be run until an advanced stage of wave overturning. A detailed analysis of wave profiles and wave kinematics (both on the free surface and within the flow) is carried out. As expected, the bottom topography is found to be an important factor controlling wave transformations and inducing three-dimensional effects on the flow. Nevertheless, comparisons of two- and three-dimensional results in the middle cross-section of the tank show remarkable similarities in jet shape and dynamics. This supports the general viewpoint that the evolution of an overturning wave becomes somewhat independent of the interior dynamics and boundary conditions.

KEY WORDS: Breaking ocean waves; nonlinear surface waves; numerical wave tank; boundary element method; three-dimensional flows; bottom topography.

INTRODUCTION

Breaking waves play a significant role in air–sea interactions, such as energy and momentum transfer from wind to water and from waves to currents, and the generation of turbulence in the upper ocean. In nearshore areas, breaking wave induced currents drive the sediment transport which leads to beach erosion and accretion. The study of breaking waves is also of importance in applications to naval hydrodynamics due to their damaging effects on ships and offshore structures in heavy seas. Due to its complexity, the process of wave breaking has not yet been fully explained. The present paper reports on numerical simulations aimed at describing the early stages of wave breaking in shallow water, namely the phenomenon of wave overturning. In particular, we concentrate on cases in which the bottom topography induces three-dimensional effects on the flow, and we restrict our study to plunging breakers which are characterized by the formation of a more prominent jet.

Most of the numerical studies of wave breaking so far have focused on two-dimensional problems. Significant contributions in the numerical simulation of steep fully nonlinear waves, based on potential flow theory, were made by Longuet-Higgins and Cokelet (1976) who developed a mixed Eulerian–Lagrangian (MEL) approach combined with a boundary integral equation (BIE) formulation. Their computations were limited to a periodic domain in deep water and they were able to reproduce overturning waves by specifying a localized surface pressure. Results obtained by New, McIver and Peregrine (1985), for plunging waves over constant depth, greatly contributed to our understanding of breaking wave kinematics. More recent two-dimensional models can accommodate both arbitrary waves and complex geometries. They are directly implemented in a physical space region where incident waves can be generated at one extremity and reflected, absorbed or radiated at the other extremity (e.g. Grilli and Subramanya, 1996; Grilli and Horrillo, 1997). For these reasons, they are often referred to as numerical wave tanks (NWT).

Only a few attempts, however, have been made for extending the numerical simulations to three dimensions, due to the more difficult geometric representation and the limitations of computer power. Xü and Yue (1992) and Xue et al. (2001) calculated three-dimensional overturning waves in a doubly periodic domain with infinite depth (i.e. only the free surface is discretized). They used a high-order quadratic boundary element method (BEM) to solve the equations in the MEL formulation. As in Longuet-Higgins and Cokelet (1976), the initial conditions were progressive Stokes waves and a localized surface pressure was applied to make waves break. Recently, Grilli, Guyenne and Dias (2001) proposed an accurate three-dimensional NWT for the description of strongly nonlinear waves over complex bottom topography. It is based on a MEL explicit time stepping and a high-order BEM with third-order spatial discretization ensuring local continuity of the inter-element slopes. Various applications of this NWT to nonlinear wave processes can be found in Guyenne, Grilli and Dias (2000) for the modelling of wave impact on a vertical wall, in Brandini and Grilli (2001*a*, *b*) for the modelling of freak wave generation due to directional wave focusing, and in Grilli, Vogelmann and Watts (2002) for the modelling of tsunami generation by submarine mass failure. In the present paper, the breaking of a solitary wave over a sloping ridge is investigated in detail using the model of Grilli et al. (2001).

In the following section, the mathematical formulation of the wave model is presented. A local regridding technique is introduced to track the wave motion far beyond the breaking point, allowing the kinematics

of a well-developed plunging wave to be examined. The case of a solitary wave propagating and overturning over a sloping ridge is analyzed in the last section. Results are obtained for the velocity and acceleration fields both on the free surface and within the flow.

MATHEMATICAL FORMULATION

Governing Equations

Equations for a fully nonlinear potential flow with a free surface are listed below. The velocity potential $\phi(\mathbf{x}, t)$ is introduced to describe an inviscid irrotational flow in Cartesian coordinates $\mathbf{x} = (x, y, z)$ with z the vertical upward direction ($z = 0$ at the undisturbed free surface), and the fluid velocity is expressed as $\mathbf{u} = \nabla\phi$.

The continuity equation in the fluid domain $\Omega(t)$ with boundary $\Gamma(t)$ is Laplace's equation

$$\nabla^2\phi = 0\,. \tag{1}$$

The corresponding three-dimensional free-space Green's function is defined as

$$G(\mathbf{x}, \mathbf{x}_l) = \frac{1}{4\pi r} \quad \text{with} \quad \frac{\partial G}{\partial n}(\mathbf{x}, \mathbf{x}_l) = -\frac{1}{4\pi}\,\frac{\mathbf{r}\cdot\mathbf{n}}{r^3}\,, \tag{2}$$

where $r = |\mathbf{r}| = |\mathbf{x} - \mathbf{x}_l|$ is the distance from the source point $\mathbf{x}$ to the field point $\mathbf{x}_l$ (both on boundary Γ), and $\mathbf{n}$ is the outward unit vector normal to the boundary at point $\mathbf{x}$

Green's second identity transforms (1) into the BIE

$$\alpha(\mathbf{x}_l)\phi(\mathbf{x}_l) = \int_\Gamma \left[\frac{\partial\phi}{\partial n}(\mathbf{x})G(\mathbf{x}, \mathbf{x}_l) - \phi(\mathbf{x})\frac{\partial G}{\partial n}(\mathbf{x}, \mathbf{x}_l)\right] \mathrm{d}\Gamma\,, \tag{3}$$

where $\alpha(\mathbf{x}_l) = \frac{1}{4\pi}\theta_l$ and θ_l is the exterior solid angle at point $\mathbf{x}_l$.

The boundary is divided into various parts satisfying different boundary conditions. On the free surface, ϕ satisfies the nonlinear kinematic and dynamic boundary conditions in the MEL formulation, respectively

$$\frac{D\mathbf{R}}{Dt} = \mathbf{u} = \nabla\phi\,, \tag{4}$$

$$\frac{D\phi}{Dt} = -gz + \frac{1}{2}\nabla\phi\cdot\nabla\phi - \frac{p}{\rho}\,, \tag{5}$$

with $\mathbf{R}$ being the position vector of a fluid particle on the free surface, g the acceleration due to gravity, p the atmospheric pressure, ρ the fluid density and $D/Dt = \partial/\partial t + \nabla\phi\cdot\nabla$ the Lagrangian time derivative. The effects of surface tension are neglected.

Here, we directly specify at $t = 0$ on the free surface, the shape $z = \eta_0(x, y)$, potential $\phi_0(x, y)$ and normal velocity $\partial\phi_0(x, y)/\partial n$ of the incident wave. On the bottom and other fixed parts of the boundary, a no-flow condition is prescribed as

$$\frac{\partial\phi}{\partial n} = 0\,. \tag{6}$$

Solution for Interior Points

Once the BIE (3) is solved, the solution within the domain can be easily evaluated from the boundary values. Using (3), the internal velocity is given by

$$\begin{aligned}\mathbf{u}(\mathbf{x}_l) = \nabla\phi(\mathbf{x}_l) \quad = \quad & \int_\Gamma \left[\frac{\partial\phi}{\partial n}(\mathbf{x})\mathbf{Q}(\mathbf{x}, \mathbf{x}_l)\right. \\ & \left. - \phi(\mathbf{x})\frac{\partial\mathbf{Q}}{\partial n}(\mathbf{x}, \mathbf{x}_l)\right] \mathrm{d}\Gamma\,,\end{aligned} \tag{7}$$

with

$$\mathbf{Q}(\mathbf{x}, \mathbf{x}_l) = \frac{1}{4\pi r^3}\mathbf{r}\,, \tag{8}$$

$$\frac{\partial\mathbf{Q}}{\partial n}(\mathbf{x}, \mathbf{x}_l) = \frac{1}{4\pi r^3}\left[\mathbf{n} - 3(\mathbf{r}\cdot\mathbf{n})\frac{\mathbf{r}}{r^2}\right]\,, \tag{9}$$

and r denoting the distance from the boundary point $\mathbf{x}$ to the interior point $\mathbf{x}_l$.

Similarly, one can also obtain the internal Lagrangian acceleration

$$\frac{D\,\mathbf{u}}{D\,t} = \frac{D\,\nabla\phi}{D\,t} = \frac{\partial\nabla\phi}{\partial t} + (\nabla\phi\cdot\nabla)\nabla\phi\,, \tag{10}$$

where the first term in the right-hand side, corresponding to the local acceleration, is given by

$$\begin{aligned}\nabla\frac{\partial\phi}{\partial t}(\mathbf{x}_l) \quad = \quad & \int_\Gamma \left[\frac{\partial^2\phi}{\partial t\partial n}(\mathbf{x})\mathbf{Q}(\mathbf{x}, \mathbf{x}_l)\right. \\ & \left. - \frac{\partial\phi}{\partial t}(\mathbf{x})\frac{\partial\mathbf{Q}}{\partial n}(\mathbf{x}, \mathbf{x}_l)\right] \mathrm{d}\Gamma\,,\end{aligned} \tag{11}$$

and the last term is computed using (7) and differentiating $\nabla\phi$. This requires calculating the spatial derivatives for all components of $\mathbf{Q}$ and $\partial\mathbf{Q}/\partial n$. Their expressions are

$$\frac{\partial Q_i}{\partial x_j} = \begin{cases} \frac{3}{4\pi r^5} r_i r_j\,, & i \neq j \\ \frac{1}{4\pi r^3}\left(\frac{3}{r^2}r_i^2 - 1\right)\,, & i = j\,. \end{cases} \tag{12}$$

$$\begin{aligned}\frac{\partial}{\partial x_j}\left(\frac{\partial Q}{\partial n}\right)_i \quad = \quad & \begin{cases} \frac{3}{4\pi r^5}\left[r_j n_i + r_i n_j - \frac{5}{r^2}(\mathbf{r}\cdot\mathbf{n})r_i r_j\right]\,, \\ i \neq j \end{cases} \\ = \quad & \begin{cases} \frac{3}{4\pi r^5}\left[\mathbf{r}\cdot\mathbf{n} + 2r_i n_i - \frac{5}{r^2}(\mathbf{r}\cdot\mathbf{n})r_i^2\right]\,, \\ i = j\,. \end{cases}\end{aligned} \tag{13}$$

where i, j refer to the spatial dimensions and r_i stands for the i-th component of $\mathbf{r}$.

The quantities $\partial\phi/\partial t$ and $\partial^2\phi/\partial t\partial n$ in (11) also satisfy a BIE similar to (3) for ϕ and $\partial\phi/\partial n$. Actually, the calculation of their values on the free surface is done as part of the second-order time integration method outlined below. Note that the results presented here are restricted to a no-flow condition on all lateral boundaries. For the use of 'snake' flap wavemaker and absorbing piston boundaries at extremities of the NWT, the reader is referred to Brandini and Grilli (2001*a*, *b*) and Grilli et al. (2002).

NUMERICAL METHOD

Time Integration

A second-order explicit scheme based on Taylor series expansions is used to update the position $\mathbf{R}$ and velocity potential ϕ on the free surface, as

$$\mathbf{R}(t + \Delta t) = \mathbf{R} + \Delta t\frac{D\,\mathbf{R}}{D\,t} + \frac{\Delta t^2}{2}\frac{D^2\mathbf{R}}{Dt^2} + O\left(\Delta t^3\right)\,, \tag{14}$$

$$\phi(t + \Delta t) = \phi + \Delta t\frac{D\,\phi}{D\,t} + \frac{\Delta t^2}{2}\frac{D^2\phi}{Dt^2} + O\left(\Delta t^3\right)\,, \tag{15}$$

where Δt is the varying time step and all terms in the right-hand sides are evaluated at time t. The time step Δt in (14) and (15) is adaptively selected at each time as

$$\Delta t = C_0\frac{\Delta r^{\min}}{\sqrt{gh}}\,, \tag{16}$$

where C_0 denotes the Courant number, $\Delta r^{\min}$ is the instantaneous minimum distance between two neighbouring nodes on Γ_f and h is a characteristic depth.

Global accuracy of the numerical scheme can be assessed at any time by checking the conservation of volume

$$V = \int_\Gamma z n_z \, \mathrm{d}\Gamma \,, \tag{17}$$

and total energy

$$E = \frac{1}{2}\rho \int_\Gamma \left(\phi \frac{\partial \phi}{\partial n} + g z^2 n_z \right) \mathrm{d}\Gamma \,, \tag{18}$$

where the first and second terms represent the kinetic and potential contributions of the flow respectively, and n_z is the vertical component of the unit normal vector.

Boundary Discretization

A high-order BEM is used to solve numerically the BIEs for ϕ and $\partial\phi/\partial t$. The boundary is discretized into collocation nodes, defining two-dimensional elements for local interpolations of the solution in between these nodes. Thus, within each element, the boundary geometry and field variables are interpolated using polynomial shape functions. Generally, isoparametric elements can provide a high-order approximation within their area of definition but only offer $\mathcal{C}^0$ continuity of the geometry and field variables at nodes in between elements. A robust treatment requires to define elements which are both high-order within their area of definition and at least locally $\mathcal{C}^2$ continuous at their edges. For this purpose, an extension of the so-called middle-interval-interpolation (MII) method introduced by Grilli & Subramanya (1996) has been developed in the three-dimensional model. The boundary elements are 4×4-node quadrilaterals associated with bi-cubic shape functions. The discretized boundary integrals are evaluated for each collocation node by numerical integration. A special treatment based on a new method of singularity extraction is applied for weakly singular integrals. As the linear algebraic system resulting from the discretization of the BIE (3) is in general dense and non-symmetric, a generalized minimal residual (GMRES) algorithm with preconditioning is used to solve it.

Regridding Techniques

Two types of regridding techniques for nodes on the free surface have been implemented. When the free surface is still single-valued, a two-dimensional regridding to a higher resolution can be performed in selected areas. It consists in specifying new equally spaced elements at a given time by reinterpolating nodes in both x- and y-directions. This offers the possibility of refining the mesh only when it becomes necessary to resolve larger variation or smaller scales of the solution.

In the MEL formulation, situations of quasi-singular integrals (when r in (3) is not zero but very small due to the inter-node proximity) are likely to occur and lead to a loss of accuracy of integrations, and eventually to numerical instabilities if the treatment of these quasi-singular integrals is not accurate enough. To overcome this difficulty, we have extended to our three-dimensional NWT the local regridding technique of Grilli and Subramanya (1996), which adaptively redistributes nodes at constant arclength intervals. More specifically, when the distance between two nodes on grid lines along the direction of wave propagation becomes too small as compared to that between neighbouring nodes (say by a factor $\frac{1}{4}$), a local regridding is carried out to make these distances equal. Grilli and Subramanya (1996) carried out two-dimensional simulations up to impact of the plunging jet on the free surface by using local regridding. It turns out that the direct extension of their technique is not as efficient here and fails to yield reliable results on the very last stages of the overturning process. This is likely because this local regridding technique slightly alters the smooth transverse variation of node distribution on the free surface, leading to small inaccuracies in the transition zones between regridded and non-regridded nodes where elements can be very distorted.

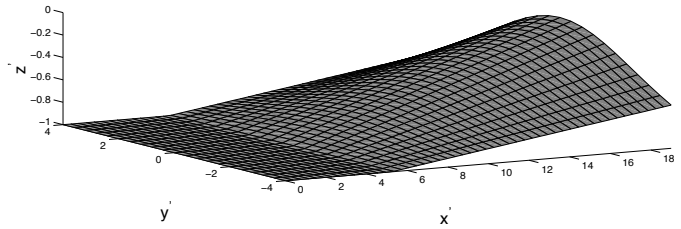

Fig. 1: Bottom topography for the shoaling of a solitary wave over a ridge modelled as a 1 : 15 slope with a lateral sech^2 modulation.

NUMERICAL RESULTS

Solitary Wave Shoaling and Breaking over a Sloping Ridge

For the purpose of inducing three-dimensional breaking, we specify a somewhat idealized sloping bottom topography in our NWT. As shown in Fig. 1, the water depth is constant in the first part of the tank ($h = h_0$). A sloping ridge starts at $x' = 5.225$, with a 1 : 15 slope in the middle cross-section and a transverse modulation of the form $\mathrm{sech}^2(ky')$ ($k = 0.25$). The computational domain is of width $8h_0$ in the y-direction and is truncated at $x' = 19$ in the x-direction. Primes hereafter indicate non-dimensional variables based on long wave theory, i.e. lengths are divided by the reference depth h_0 and times by $\sqrt{h_0/g}$. The initial condition is a numerically exact solitary wave of potential flow theory (Tanaka, 1986), with height $H_0' = 0.6$ and its crest initially located at $x' = 5.7$. The initial discretization consists of $50 \times 20 \times 4$ quadrilateral elements in the x-, y- and z-directions respectively ($\Delta x_0' = 0.38$, $\Delta y_0' = 0.4$, $\Delta z_0' = 0.25$). The total number of nodes is $N_\Gamma = 2862$ and the initial time step is set to $\Delta t_0' = 0.171$ for $C_0 = 0.45$. The computation is first performed in the initial discretization as long as errors remain acceptable (i.e. less than 0.05% or so on wave mass and energy). A two-dimensional regridding to a finer resolution is then applied at $t' = 5.851$ for which errors on volume and energy conservation are 0.012% and 0.032% respectively. The discretization is increased to $60 \times 40 \times 4$ quadrilateral elements in the portion $8 \le x' \le 19$ ($\Delta x' = 0.18$, $\Delta y' = 0.2$, $N_\Gamma = 6022$).

As the solitary wave travels up the sloping ridge, it loses the initial vertical symmetry and develops a very steep forward face. The transformation is more pronounced in the middle of the tank ($y' = 0$) where the water depth is the least. The three-dimensional wave profile in advanced stages of wave overturning is shown in Fig. 2. As the overturning process propagates laterally to the sidewalls ($y' = \pm 4$), the projected water forms a sharp tongue-shaped jet, which is obviously a three-dimensional effect. We used the local regridding technique to reduce the occurrence of quasi-singularities due to node convergence in the breaker jet. However, the computation cannot be pursued much beyond $t' = 8.965$ because the elements become too distorted. The CPU time for $N_\Gamma = 6022$ is currently $O(7)$ minutes per time step on a single processor of a NEC SX5 supercomputer. It should be emphasized that no smoothing/filtering was used to stabilize the solution.

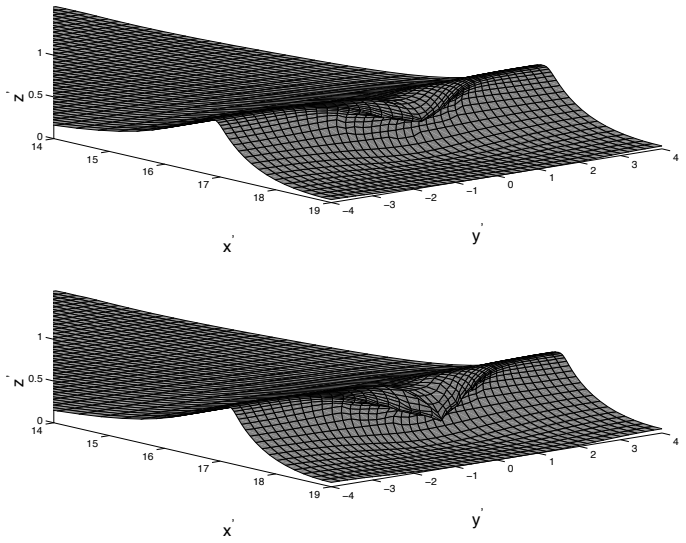

Fig. 2: Wave profiles at $t' = 8.757$ (upper) and $t' = 8.965$ (lower).

Fig. 3 displays the vertical cross-sections of the free surface in the middle ($y' = 0$) and at the sidewalls ($y' = \pm 4$) for times $t' = 7.911$, 8.255, 8.502, 8.757 and 8.965. Due to the depth difference, one can see that the wave profile at $y' = 0$ has developed overturning with a prominent jet while the profile at $y' = \pm 4$ remains single-valued. The wave reaches its maximum height $H' \simeq 0.71$ near the breaking point ($t' = 7.911$) with its crest located at $x' = 16.2$.

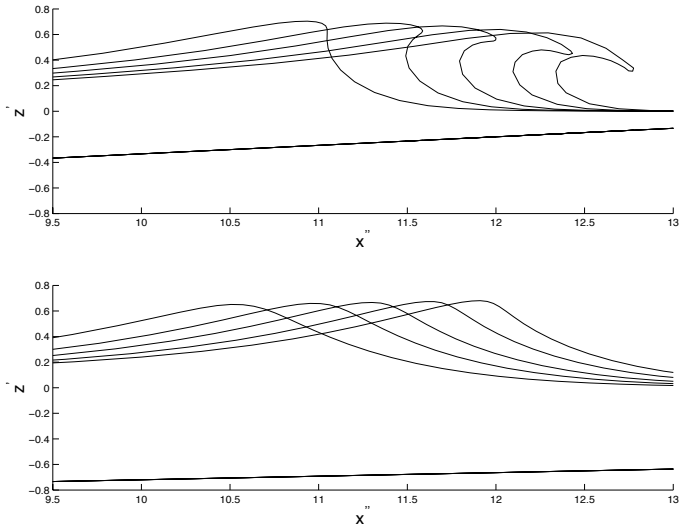

Fig. 3: Vertical cross-sections at $y' = 0$ (upper) and $y' = \pm 4$ (lower) for $t' = 7.911$, 8.255, 8.502, 8.757 and $t' = 8.965$.

Fig. 4 and 5 show a comparison of free surface profiles using the two-dimensional model of Grilli et al. (1997) and the present three-dimensional model for the same experimental parameters. At a given time, the crests of both two- and three-dimensional waves are roughly located at the same position. However, in Fig. 4, we see that wave breaking occurs earlier in two dimensions. This observation can be explained by differences in wave evolution between the middle and the sides of the tank. Thus, near sidewalls, the wave is less affected due to the deeper bottom. This somewhat delays the overturning process in the middle part of the tank. Fig. 5 presents a comparison for slightly different times, at which the two- and three-dimensional waves exhibit similar free surface profiles. Furthermore, to allow for a direct comparison of breaker jet geometry, the two-dimensional profile is shifted forward to make it approximately coincide with the three-dimensional profile. The breaker jet of the three-dimensional wave almost perfectly coincides with that of the two-dimensional wave. Careful examination reveals that the three-dimensional wave has a higher back slope and a more arched front face than for the two-dimensional case.

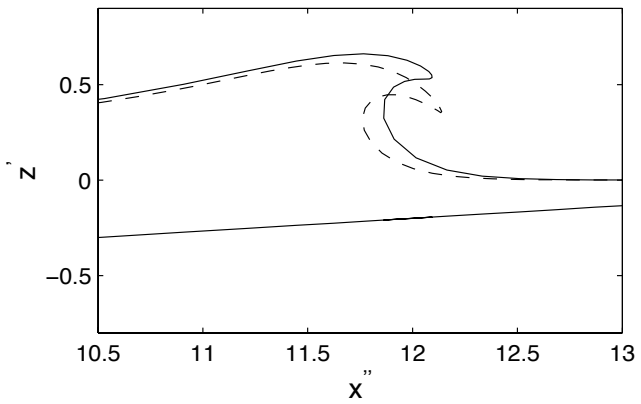

Fig. 4: Wave profiles at $t' = 8.55$ using the two-dimensional model of Grilli et al. (1997) (dashed line) and the present three-dimensional model at $y' = 0$ (solid line).

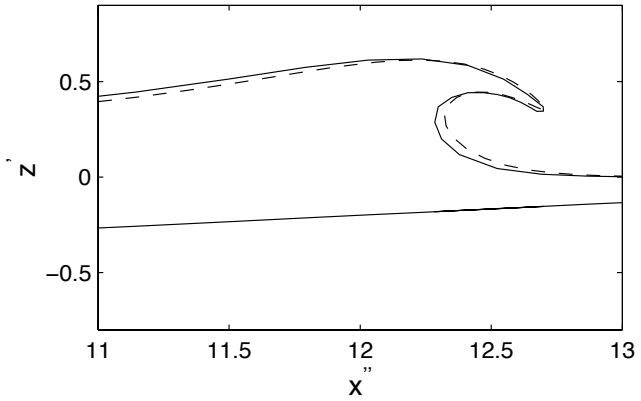

Fig. 5: Comparison of two-dimensional (dashed line) and three-dimensional (solid line) results at the same stage of overturning: $t' = 8.560$, 8.920 for the two-, three-dimensional wave.

Kinematics of Three-Dimensional Overturning Waves

We address now the effects of three-dimensional breaking on the wave kinematics. Fig. 6 shows the surface velocity and acceleration fields (u_x, u_z) and (a_x, a_z) in the middle of the tank ($y' = 0$). As the wave crest overturns, the particle velocity increases and is almost twice $c = \sqrt{gh_0}$ near the tip of the plunging jet at $t' = 8.965$. It can be seen that acceleration magnitudes as high as almost six times g occur at $t' = 8.965$ on the front face where the curvature is large. As one approaches the tip of the jet, accelerations close to g indicate the tendency to a free fall motion.

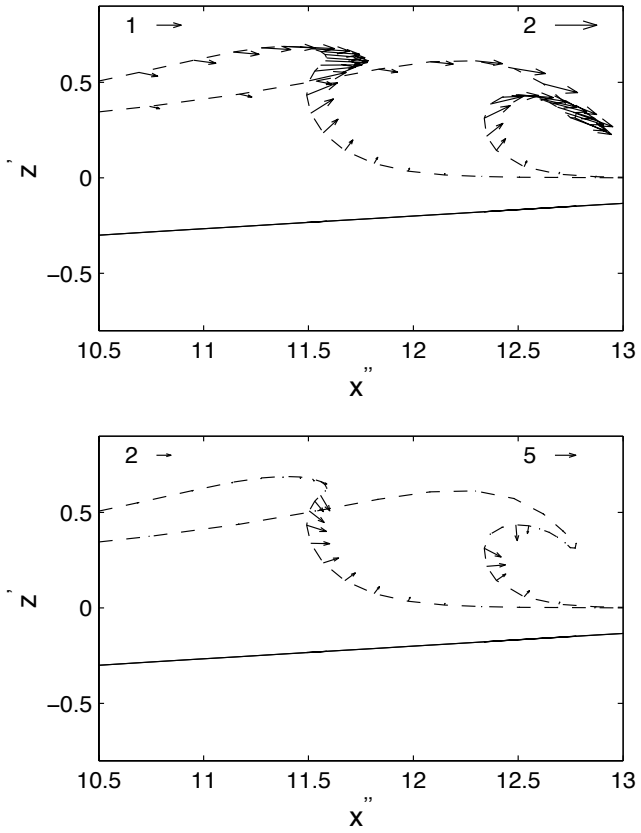

Fig. 6: Vertical cross-sections of the surface velocity (upper) and acceleration (lower) field at $y' = 0$ for $t' = 8.255, 8.965$.

Fig. 7 displays the internal velocity and acceleration fields (u_x, u_z) and (a_x, a_z) in the middle of the tank ($y' = 0$) at $t' = 8.965$. Outside the overturning region, the quasi-uniformity of the velocity distribution is clearly shown. The velocity increases and exhibits more variation in the vertical direction as one enters the breaker jet. In contrast, the corresponding acceleration field (a_x, a_z) has appreciable values only in the region adjacent to the wave front face. Further examination reveals that a transition zone takes place beneath the back slope of the wave, more precisely at $x' \simeq 11.9$ ($t' = 8.965$), between low backward accelerations and high forward accelerations. The location of this transition zone coincides with the location of the wave crest at $y' = \pm 4$ which has not overturned yet.

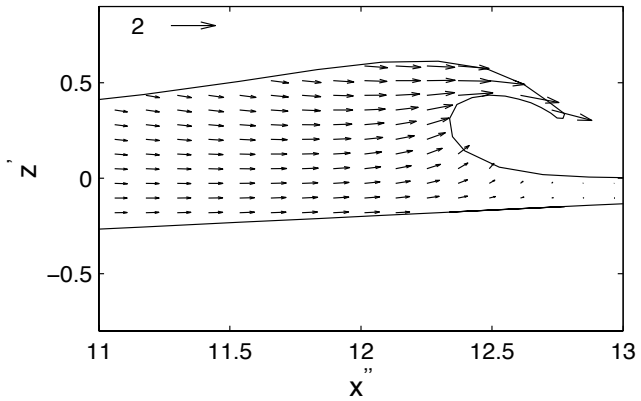

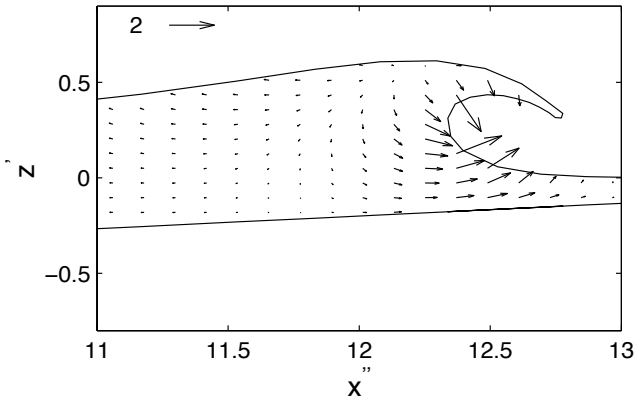

Fig. 7: Vertical cross-sections of the internal velocity (upper) and acceleration (lower) field at $t' = 8.965$. In the (z, x)-plane, the maximum velocity (acceleration) magnitude is $|\mathbf{u}'|_{\max} = 1.918$ ($|\mathbf{a}'|_{\max} = 2.474$).

The transverse variation of the wave kinematics is illustrated in Fig. 8 where we plot the internal velocity and acceleration fields (u_x, u_y) and (a_x, a_y), in a horizontal cross-section at depth $h' = -0.2$ and time $t' = 8.965$. As indicated, the propagation of the solitary wave is associated with a forward displacement of water beneath the surface. The wave-induced velocity and acceleration fields are appreciable only in the vicinity of the wave crest position. A remarkable feature is that the fluid motion remains primarily longitudinal but there are small transverse variations due to focusing of the flow by the ridge. The transition zone, as mentioned earlier, between small negative accelerations and large positive accelerations is clearly represented by a transverse dotted line.

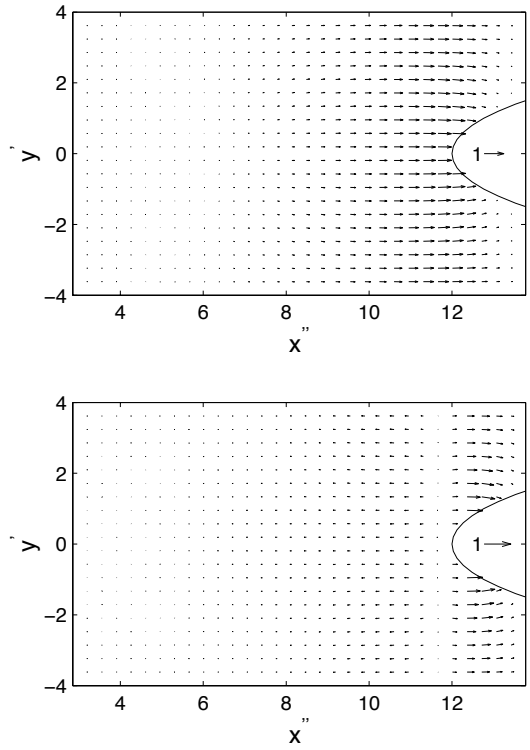

Fig. 8: Horizontal cross-sections of the internal velocity (upper) and acceleration (lower) field at depth $h' = -0.2$ and $t' = 8.965$. In the (x, y)-plane, the maximum velocity (acceleration) magnitude is

$|\mathbf{u}'|_{\max} = 0.683$ ($|\mathbf{a}'|_{\max} = 0.580$). The ratio of maximum $|u_x|$ ($|a_x|$) to maximum $|u_y|$ ($|a_y|$) is $|u_x/u_y|_{\max} = 8.9$ ($|a_x/a_y|_{\max} = 6.5$).

Three-dimensional effects are especially conspicuous in Fig. 9 which shows the internal velocity field (u_y, u_z) and the corresponding acceleration field (a_y, a_z). Components u_z and a_z decrease rapidly with z, attaining negligible values near the bottom and near the sidewalls where depth is the greatest. This is a typical effect in shallow water, which results from the flattening of the orbital motion of fluid particles near the bottom. The development of wave breaking is indicated by the flow convergence above the top of the ridge, and by the decay of velocities just beneath the surface as one tends laterally to $y' = 0$. As wave breaking develops, variations of a_y become more and more significant with values comparable to those of a_z in the upper region just behind the plunging jet. Thus, the kinematics of three-dimensional overturning waves is characterized by a strong energy and momentum transfer from the vertical to transverse motion.

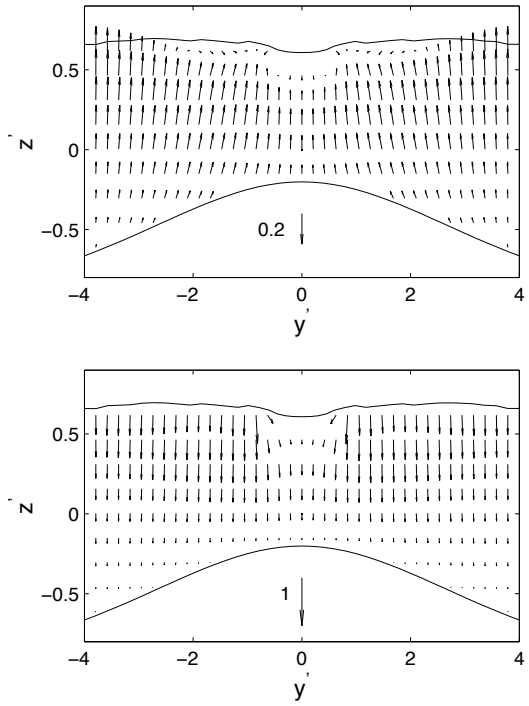

Fig. 9: Transverse vertical cross-sections of the internal velocity (upper) and acceleration (lower) field at $t' = 8.965$ ($x' = 17.2$). In the (y, z)-plane, the maximum velocity (acceleration) magnitude is $|\mathbf{u}'|_{\max} = 0.172$ ($|\mathbf{a}'|_{\max} = 0.613$). The ratio of maximum $|u_z|$ ($|a_z|$) to maximum $|u_y|$ ($|a_y|$) is $|u_z/u_y|_{\max} = 2.7$ ($|a_z/a_y|_{\max} = 1.8$).

CONCLUSIONS

The three-dimensional NWT of Grilli et al. (2001) has been used to investigate the shoaling and overturning of a solitary wave over a sloping ridge with a lateral modulation. A local regridding technique has been developed to allow computations to be pursued until an advanced stage of overturning. We focused on the case of a plunging breaker and performed a detailed analysis of its dynamics and kinematics. Comparisons between two- and three-dimensional results for similar parameters have been carried out. Overall, the corresponding wave profiles at $y' = 0$ are found to be almost identical, particularly near the plunging jet, but breaking is found to occur for slightly different times and x-locations. Moreover, results for maximum velocity and acceleration computed near the three-dimensional breaking jet (at $y' = 0$) are consistent in magnitude and direction with the two-dimensional results reported by New et al. (1985) for plunging breakers over constant depth. Such similarities in near jet shape and dynamics of two- and three-dimensional plunging waves seems to indicate that the flow near breaking jets in the latest stages of overturning somewhat becomes independent of the background flow and boundary conditions (including shape of the sloping bottom), which have led to breaking.

ACKNOWLEDGEMENTS

S.T. Grilli acknowledges support from the US National Science Foundation, under grant CMS-0100223 of "the Engineering/Earthquake, Hazards and Mitigation Program". Computations carried out in this research project were performed in part on the NEC SX5 supercomputer located at IDRIS.

REFERENCES

Brandini, C. and S.T., Grilli (2001a). "Modelling of freak wave generation in a three-dimensional NWT," *Proc. 11th Intl Offshore and Polar Engng Conf.*, Stavanger, Norway.

Brandini, C. and S.T., Grilli (2001b). "Three-dimensional wave focusing in fully nonlinear wave models," *Proc. 4th Intl Symp. on Ocean Wave Measurement and Analysis*, San Francisco, USA, pp. 1102-1111, ASCE.

Grilli, S.T., Guyenne, P. and F., Dias (2001). "A fully nonlinear model for three-dimensional overturning waves over arbitrary bottom," *Intl J. Numer. Meth. Fluids*, Vol 35, pp. 829-867.

Grilli, S.T. and J. Horrillo (1997). "Numerical generation and absorption of fully nonlinear periodic waves," *J. Engng. Mech.*, Vol 123(10), pp 1060-1069.

Grilli, S.T. and R., Subramanya (1996). "Numerical modeling of wave breaking induced by fixed or moving boundaries," *Computational Mech.*, Vol 17, pp 374-391.

Grilli, S.T., Svendsen, I.A. and R., Subramanya (1997). "Breaking criterion and characteristics for solitary waves on slopes," *J. Waterway Port Coastal and Ocean Engng.*, Vol 123(3), pp 102-112.

Grilli, S.T., Vogelmann, S. and P., Watts (2002). "Development of a three-dimensional numerical wave tank for modelling tsunami generation by underwater landslides," *Engng Anal. Boundary Elem.*, Vol 26, pp. 301-313.

Longuet-Higgins, M.S. and E.D., Cokelet (1976). "The deformation of steep surface waves on water. I. A numerical method of computation," *Proc. R. Soc. Lond.* A, Vol 350, pp. 1-26.

New, A.L., McIver, P. and D.H. Peregrine (1985). "Computations of overturning waves," *J. Fluid Mech.*, Vol 150, pp. 233-251.

Tanaka, M. (1986). "The stability of solitary waves," *Phys. Fluids*, Vol 29, pp. 650-655.

Xü, H. and D.K.P., Yue (1992). "Computations of fully nonlinear three-dimensional water waves," *Proc. 19th Symp. on Naval Hydrodynamics*, Seoul, Korea.

Xue, M., Xü, H., Liu, Y. and D.K.P., Yue (2001). "Computations of fully nonlinear three-dimensional wave–wave and wave–body interactions Part 1. Dynamics of steep three-dimensional waves," *J. Fluid Mech.*, Vol 438, pp. 11-39.